

MAGNETIC CHANGES IN THE COURSE OF THE X7.1 SOLAR FLARE ON 2005 JANUARY 20

JINGXIU WANG, MENG ZHAO, AND GUIPING ZHOU

National Astronomical Observatories, Chinese Academy of Science, Beijing 100012, China

Received 2008 April 12; accepted 2008 September 9; published 2008 December 1

ABSTRACT

Rapid magnetic changes in the course of the X7.1 solar flare on 2005 January 20 at the photosphere in the host active region (AR), NOAA AR 10720, are diagnosed. The database for this study consists of Huairou vector magnetograms, *Transition Region and Coronal Explorer* (TRACE) white light and UV/EUV images, RHESSI hard X-ray, and *Solar and Heliospheric Observatory* EUV observations. For such an event that is close to but not on the solar west limb (N12 W58), the projection effects in the observed vector magnetograms are untangled by combining an intuitive geometric analysis and a transformation of the magnetograms into the heliographic coordination system. The magnetic changes in the horizontal magnetic fields are emphasized. We find definitive evidence of weakening in the horizontal magnetic fields in a few isolated patches in the outskirts of this δ -sunspot group and strengthening in the horizontal fields (HFs) in an extended area centralized at the magnetic neutral line between major sunspots of opposite polarities. The rapid magnetic changes take place at the level of 100–300 G, several factors of ten of the noise level. The identified HF changes are consistent with the darkening of inner penumbrae and weakening of outer penumbrae in this δ -sunspot group. The enhanced HFs spatially coincide with the TRACE 1550 Å rope-like structures lying low above the magnetic neutral line. Unexpectedly, during the flare, the lower lying rope-like structures remain in place, though they exhibit episodic disturbance and brightening, while the outer EUV loops are impulsively expanding. The rapid magnetic changes manifest an impulsive input of free magnetic energy in the photosphere, resulting from an impulsive growth of a new emerging flux region (EFR) along the magnetic neutral line. The facts of the increasing core fields in magnetic nonpotentiality, the continued disturbance of the inner rope-like structures, and the breakout of the outer loops during the major flare cannot be interpreted by any single flare model. However, the nature of magnetohydrodynamical catastrophe is clearly implied for the flare triggering.

Key words: Sun: coronal mass ejections (CMEs) – Sun: flares – Sun: magnetic fields

Online-only material: color figures

1. INTRODUCTION

The flare-associated changes in magnetic fields have been a long-standing issue in solar physics. This comes from a need to understand the physics of magnetic energy storage and explosive release in the solar atmosphere. Magnetic activity, like solar flares, takes place in stars and other astrophysical environments. The understanding of flare energetics would lead to a fundamental improvement of our knowledge about explosive phenomena in general astrophysics.

An immediate purpose of studying the flare-associated changes in magnetic fields is to examine various flare models that have been developed over many decades of studies. It is well known that the energy released in flares comes from the free energy previously stored in the magnetic fields, and the eruptive nature of energy release results from an explosive conversion of magnetic energy, presumably by means of magnetic reconnection, into other forms of energy to accelerate energetic particles and heat the solar atmosphere.

The general issue of flare-associated magnetic changes can be grossly divided into three interconnected topics: (1) gradual magnetic evolution leading to flares, (2) rapid magnetic changes in the course of flares, and (3) flare-induced signals in observations by the profile changes of spectral lines used in polarization measurements.

The first topic is often referred to as the study of the pre-flare state or flare energy buildup. This type of study goes back as early as the 1930s (Giovannelli 1939), and has been reviewed by many authors (Rust 1976; Švestka 1981; Gaizauskas &

Švestka 1987; Rust et al. 1994; Sakurai & Hiei 1996). Wang (1998) summarized the following seven conditions that favor flare occurrence.

1. Strongly curved magnetic neutral lines, e.g., “S” or reverse “S” shaped (Somov 1985);
2. Steep gradients of line-of-sight (LOS) magnetic fields, i.e., several hundred G per kilometer (Wang & Li 1998);
3. Filament activation, e.g., darkening, bifurcating, and twisting (Ramsey & Smith 1963; Rust et al. 1994);
4. Emerging flux regions (EFRs; Bruzek 1967; Zirin 1972), often being pre-stressed, particularly within great δ -sunspots (Zirin 1988), and/or in an activity center of active regions (Bumba 1987);
5. Highly sheared transverse (TRS) fields, which are measured by the shear angle of vector magnetic fields (Hagyard et al. 1984; Lü et al. 1993), field strength, and the extent of strong shear;
6. Magnetic flux cancelation (Livi et al. 1985; Martin et al. 1985), particularly when one component of a canceling magnetic feature (CMF) comes from an EFR (Wang & Shi 1993);
7. Vertical current concentration (Moreton and Severny 1968; Lin & Gaizauskas 1987; Ding et al. 1987), often unneutralized and with a maximum magnitude of several times 10^4 A km⁻² (Canfield et al. 1993; Wang et al. 1996).

More recent studies can be found in the references in Falconer et al. (2006), Leka & Barnes (2007), Schrijver (2007), and Kubo et al. (2007).

The rapid magnetic changes in the course of flares were first reported by Patterson & Zirin (1981) in terms of a “flare-transient” based on an analysis of Big Bear LOS magnetograms. It was soon recognized that the reported flare transients are not real but produced by transient emission of the Fe I 5324 Å line used for obtaining magnetograms (Patterson 1984). The earlier report from Patterson & Zirin (1981) was just flare-induced signals in polarization measurements.

Further stimulation to the relevant studies came from the report of Kosovichev & Zharkova (1999) from an analysis of magnetograms obtained by the Michelson Doppler Imager (MDI; Scherrer et al., 1995) on board *Solar and Heliospheric Observatory* (SOHO). For an X5.6 flare on 2001 April 6, Qiu & Gary (2003) provided a scenario that the observed transient polarity reversal in MDI magnetograms is likely to be produced by distorted measurements when the Ni I 6768 Å line comes into emission or strong central reversal as a result of nonthermal beam impact on the atmosphere in regions of strong magnetic fields. They called this transient polarity reversal a “magnetic anomaly.” Nonlocal thermodynamic equilibrium (LTE) radiative transfer calculations (Ding et al. 2002) confirmed the interpretations of Kosovichev & Zharkova (2001) and Qiu & Gary (2003). Kosovichev & Zharkova (2001) detected two types of rapid magnetic changes associated with the Bastille Day flare/coronal mass ejection (CME) event: irreversible changes and magnetic transients. More detailed studies on the so-called magnetic anomaly would be of interest not only for a clear distinction between true magnetic changes in flares and flare-induced signals in polarization measurements, but also for understanding the processes of flare energetics.

Cameron & Sammis (1999) detected a significant change in the longitudinal magnetic fields in NOAA Active Region (AR) 6063 during an X9.3 flare. As this flare took place near the west limb (N33 N78), the observed change should be well interpreted as a change in horizontal magnetic fields. Since then, more than 30 major flares have been carefully examined, which are listed in Table 1, and convincing evidence of rapid, significant, and persistent changes in the longitudinal and TRS fields are reported. It is worthwhile to notice that the majority of the major flares in Table 1 (28 X-class and 5 M-class) are associated with halo CMEs.

Sudol & Harvey (2005) reviewed the relevant studies in the interval from 1999 to 2005 for 20 major flares with emphasis on the longitudinal field changes during flares, and presented new evidence of longitudinal magnetic field changes accompanying 15 X-class flares. They conclude the ubiquity of the abrupt, significant, and permanent changes of the photospheric longitudinal magnetic field for X-class flares, and further declare (page 656) that “one of the basic assumptions of modern flare theories (see Priest & Forbes 2002), that the photospheric magnetic field does not change during flares, needs to be reexamined.”

Rapid magnetic changes in the course of major flares do take place in horizontal magnetic fields (see the review of Wang 2007). Indeed, the horizontal field (HF) changes contain more direct information on the storage and release of free magnetic energy in ARs. The diagnosis of HF changes is made in three different ways: vector magnetogram analysis for flares close to the disk center (Flares 2, 5, 12, 13, 20, 28, 32, 33 in Table 1), LOS magnetogram analysis for limb events (Flares 1, 8, 19), and sunspot structure analysis with white-light (WL) images (Flares 4, 7, 9, 10, 12, 16, 18, 21, 28, 29, 30, 31, 33). The majority of the work has been done by Big Bear Group. The earlier reports

on the enhancement of HFs and magnetic shear after an X-class flare trace back to the 1990s (Schmieder et al. 1994; Wang et al. 1994).

The rapid penumbra decay in the outer δ -sunspots and the enhancement of inner penumbrae and central umbrae after major flares are a remarkable fact discovered by Big Bear Group (Wang et al. 2004a, 2005; Deng et al. 2005; Liu et al. 2005). Chen et al. (2007) extend these studies by including 403 flares, in which there are 40 X-class, 174 M-class, and 189 C-class flares. It is found that rapid and permanent structural changes are evidenced in the time profile of WL mean intensity and are unlikely to result from flare emission. For X-class flares, over 40% of events show distinct sunspot structure changes, while for M-class and C-class flares, this percentage drops to 17% and 10%, respectively.

For the studied events when high-quality vector magnetograms are available, evidence has been found that during the flares, there appear rapid, irreversible enhancements of the photospheric TRS magnetic field and magnetic shear at some section of the magnetic neutral line (Wang et al. 2002a, 2002b, 2004a, 2004b, 2005, 2007; Liu et al. 2005). The TRS field increases at the magnitude of 100 G, and the field-weighted shear angle at 10° . A consistent picture that the TRS field decreases in the penumbral decay area while it increases in the central darkening region has emerged by careful comparison of sunspot structure and vector magnetic field changes (Liu et al. 2005). It seems to be also true that abrupt, significant, and permanent changes of the photospheric TRS magnetic field are a ubiquitous feature of many X-class flares.

Although the rapid, significant, and permanent changes in both longitudinal and TRS fields during flares have been convincingly demonstrated, a good understanding of these changes in the frame of flare models tends to be not easily achieved. A partial reason for this is the fact that most of the flare models have not been confronted with measurements of vector magnetic fields in the photosphere. From the observational side, there are not many major flares with co-temporal observations of vector magnetograms of high spatial resolution, adequate cadence, and temporal coverage. In addition, in some of the analyses, the magnetic changes have not been put into the observed flare scenario to gain a consistent picture. More data, e.g., the dynamics of UV/EUV and X-ray loops, need to be taken in conjunction with magnetic changes.

AR 10720 rotated onto the solar disk as a simple beta magnetic sunspot on 2005 January 10 and ended as a large, magnetic complex sunspot region on 2005 January 22. In its disk transit, it grew rapidly and showed impressive activity. From 2005 January 14 to 21, it produced five X-class flares and 18 M-class flares. At 06:36 UT on 2005 January 20, an X7.1 flare exploded in AR 10720 near the northwest solar limb. The flare had its maximum phase at 07:01 UT and faded away at 07:26 UT. It was followed by an Earth-directed CME that left the Sun at a speed of approximately 882 km s^{-1} with clear acceleration. This solar event was associated with the hardest energetic proton event of Solar Cycle 23, which had the highest, $\geq 100 \text{ MeV}$, proton flux level observed since October 1989. It was also associated with the largest ground-level event in Cycle 23. Fortunately, for this superactive AR, vector magnetograms with adequate cadence and sensitivity have been obtained at Huairou Solar Observing Station (HSOS) during its whole disk transit. Thus, this great flare, amongst others, would serve as a good example for an independent examination if definitive magnetic changes could be identified in the flare

Table 1
Major Flares Which Show Rapid Magnetic Changes During Flare

	Date	Class	Remark	Reference
1	1990 May 24	X9.3	$B_{\parallel}(B_{\perp})$	Cameron & Sammis (1999)
2	1991 Mar 22	X9.0	B & Shear	Wang et al. (2002b)
3	1998 May 2	X1	B_{\parallel}	Kosovichev & Zharkova (1999)
4	2000 Jun 6	X2.3	WL	Wang et al. (2004b), Deng et al. (2005) Liu et al. (2005)
5	2000 Jul 14	X5.7	B_{\parallel} B & Shear	Kosovichev & Zharkova (2001) Wang et al. (2005)
6	2000 Nov 26	X4.0	B_{\parallel}	Meunier & Kosovichev (2003)
7	2001 Mar 10	M6.7	WL, B_{\parallel}	Li et al. (2005a)
8	2001 Apr 2	X20	$B_{\parallel}(B_{\perp})$	Spirock et al. (2002), Wang et al. (2002b) Sudol & Harvey (2005)
9	2001 Apr 6	X5.6	B_{\parallel} , WL	Wang et al. (2002b), Liu et al. (2005)
10	2001 Apr 9	M7.9	WL	Liu et al. (2005)
11	2001 Jun 23	X1.2	B_{\parallel}	Sudol & Harvey (2005)
12	2001 Aug 25	X5.3	B & Shear WL, B_{\parallel}	Wang et al. (2002b) Liu et al. (2005), Sudol & Harvey (2005)
13	2001 Oct 19	X1.6	B & Shear B_{\parallel}	Wang et al. (2002b) Sudol & Harvey (2005)
14	2001 Oct 22	X1.2	B_{\parallel}	Wang et al. (2002b), Sudol & Harvey (2005)
15	2001 Dec 11	X2.8	B_{\parallel}	Sudol & Harvey (2005)
16	2002 Feb 20	M2.4	WL, B_{\parallel}	Wang et al. (2002a)
17	2002 May 20	X2.1	B_{\parallel}	Sudol & Harvey (2005)
18	2002 Jul 15	X3.0	WL B_{\parallel}	Liu et al. (2005) Liu et al. (2003), Li et al. (2005b)
19	2002 Jul 23	X4.8	$B_{\parallel}(B_{\perp})$	Yurchyshyn et al. (2004)
20	2002 Jul 26	M8.7	B & Shear	Wang et al. (2004a)
21	2002 Jul 29	M4.7	WL	Chen et al. (2007)
22	2002 Aug 21	X1.0	B_{\parallel}	Sudol & Harvey (2005)
23	2003 May 27	X1.3	B_{\parallel}	Sudol & Harvey (2005)
24	2003 May 28	X3.6	B_{\parallel}	Sudol & Harvey (2005)
25	2003 Jun 10	X1.3	B_{\parallel}	Sudol & Harvey (2005)
26	2003 Jun 11	X1.6	B_{\parallel}	Sudol & Harvey (2005)
27	2003 Oct 26	X1.2	B_{\parallel}	Sudol & Harvey (2005)
28	2003 Oct 28	X17.2	B & Shear WL	Wang et al. (2004b) Liu et al. (2005)
29	2003 Oct 29	X10.0	WL B_{\parallel}	Wang et al. (2004b), Liu et al. (2005) Sudol & Harvey (2005)
30	2003 Nov 2	X8.3	WL, B_{\parallel}	Liu et al. (2005), Sudol & Harvey (2005)
31	2004 Jul 16	X3.6	WL	Chen et al. (2007)
32	2005 Sep 13	X1.5	B & Shear	Wang et al. (2007)
33	2006 Dec 13	X3.4	WL, B & Shear	Jing et al. (2008)

course and the characteristics of the rapid magnetic changes are known.

The X7.1 flare took place at N12 and W58, close to the solar west limb. The angle between the LOS and the local normal at the flare site is approximately 59° . For such an event, the measurements of vector magnetic fields suffered from severe projection effects. We could transform the observed vector magnetograms into the heliographic coordination system (see Gary & Hagyard 1990) to untangle the projection effect, though it is not recommended when an AR is more than 50° away from the disk center. From the poor spatial sampling and sensitivity of the observed magnetograms when the target AR was close to the solar limb, one might not be able to totally reckon on such a transformation. Intuitive geometric analysis would be a supplemental way to untangle the projection effects. On the other hand, there is an advantage when dealing with a limb event. Like the cases studied by Cameron & Sammis (1999), Spirock et al. (2002), and Yurchyshyn et al. (2004), the LOS magnetograms for events close to the limb do represent the horizontal component of the magnetic vector without serious 180° ambiguity in field azimuth. Moreover, scrutinizing the

continuous variation of the apparent field distribution in a given AR from the disk center to the limb would provide clues in learning the real distribution and geometry of vector magnetic fields.

This paper is aimed at examining whether or not rapid magnetic changes associated with such an extreme flare/CME event appear, and what we can learn about the flare magnetism and energetics from the observed magnetic changes. Efforts are made to obtain a consistent picture about the changes in magnetic fields, WL, and UV/EUV structures during the flares. Emphasis is put on the HF changes during the flare. In the next section, we describe the observations and our strategy in data analysis. The identified magnetic changes are presented in Section 3. Discussions on the implications of the identified magnetic changes for flare models are presented in the last section.

2. DATABASE AND ANALYSIS

The database for this study consists of vector magnetograms obtained with the Fe I 5324 Å line and H β filtergrams taken at HSOS, the UV 1550, 1600, 1700 Å, and WL images from

the *Transition Region and Coronal Explorer* (TRACE; Handy et al. 1999), *SOHO*/the EUV Imaging Telescope (EIT) 195 Å observations (Delaboudinière et al. 1995), and *SOHO*/MDI magnetograms. All of the images on 2005 January 20 are co-aligned with respect to the pre-flare time of 01:33 UT by solar software procedures.

The HSOS vector magnetograms used in this study are integrated by 256 pairs of images. The sensitivity for the LOS component of the vector magnetograms is better than 20 G, and for the TRS components, 150 G. It is necessary to have an acceptable resolution of 180° ambiguity of the field azimuth in the observed magnetograms. We take the assumption that the observed magnetic vector is closer to the potential configuration when selecting field azimuth from the two alternatives. Daily vector magnetograms from January 13–20 with ambiguity in field azimuth removed are shown in Figure 1. When the magnetograms are used in time sequence, seeing effects on the magnetogram sensitivity are corrected by the method described by Wang et al. (1996). The original magnetograms have a pixel size of 0.3516 arcsec. To increase the sensitivity, a 2×2 pixel smooth average has been made. The actual seeing at Huairou specifies the spatial resolution of the observations, which is about 2 arcsec.

One key characteristic of AR 10720 is the successive appearance of “sheared” EFRs. In the vector magnetograms, a remarkable manifestation of an EFR is the appearance of a bundle of enhanced TRS fields, which is often the first or even the only signature of a new EFR in observations (Wang & Shi 1993). By “sheared” it is meant that the EFRs’ opposite polarity flux emerged on both sides of the main magnetic neutral line, and separated along the neutral line in the opposite directions. The first four EFRs marked from January 13 to 15 met this definition. As a result of the successive “sheared” EFRs, the magnetic neutral line is greatly elongated with obviously enhanced magnetic shear. The four sheared EFRs resulted in a net growth of opposite polarity flux along the magnetic neutral line. They seemed to make up a big EFR of very wide separation with two apparent poles on both ends of the neutral line. The apparent negative pole indicated by the arrow in the magnetogram on January 15 moved more than 30,000 km from January 13 to 17 with an average speed close to 0.2 km s^{-1} . Until January 20, this negative flux patch can still be identified (indicated by an arrow in the last panel of Figure 1).

EFRs 5 and 6 (marked in the magnetogram of 2005 January 16) appeared in the north of the AR within areas of negative flux. Their first appearance went back to January 13, as positive-flux knots in the magnetograms. Their continuous development can be traced to January 20 as large areas of positive flux from the middle to the north of the AR, forming parts of the AR’s outskirts. The magnetic orientation of EFRs 5 and 6 is opposite to the earlier four EFRs and the main magnetic bipole of the AR, making the general topology of the AR more complicated. A few major flares in this AR, including the X7.1 flare studied in this work, have their ribbons mostly or partially covered by the area of these EFRs. The identity of the seventh EFR in the southern positive-flux region is tentative since serious projection effects appeared in the magnetograms.

In some sense, the rapid growth with different dipoles intertwined gives the impression of an eruption of a single δ -sunspot group, which was pre-twisted below the surface (Zirin & Liggett 1987).

Another key characteristic of the AR evolution is the obvious flux cancellation along the west part of the magnetic neutral line.

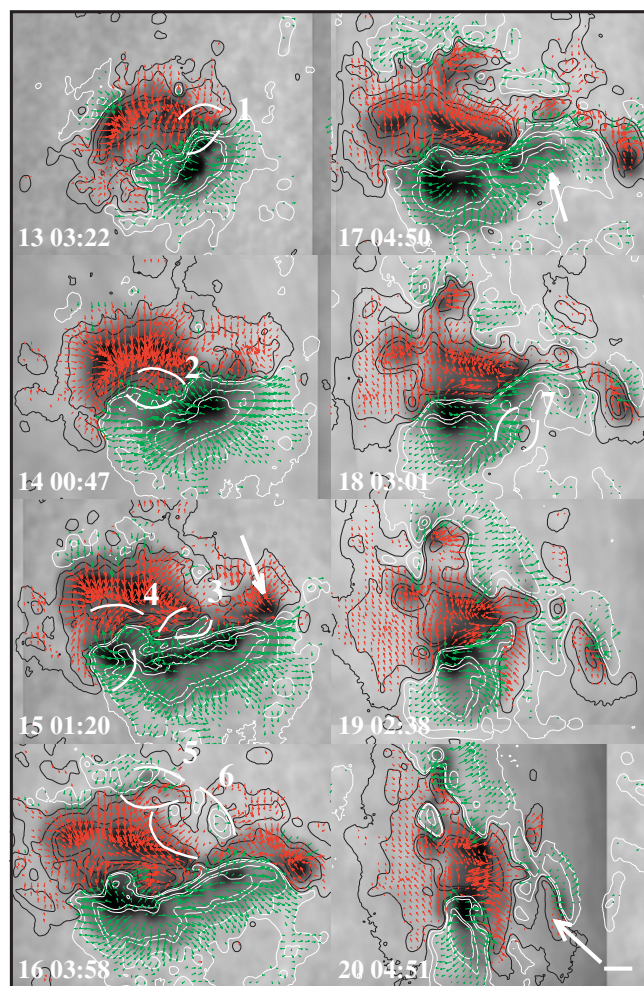


Figure 1. Daily vector magnetograms. The images are narrowband filtergrams of Fe I 5324 Å showing sunspots. The contours represent the LOS component of vector field with levels of ± 100 , 250, 500, 1000, 1500 G. White (black) contours are referred to positive (negative) polarity. The arrows represent the TRS components of the magnetic vector with length proportional to the field strength and green (red) color from positive (negative) LOS fields. Each EFR is marked by a bracket and with a number. The white bar in the lower-right corner denotes a scale of 20 arcsec, which is maintained for the other figures too.

(A color version of this figure is available in the online journal.)

An arrow in the magnetogram on 2005 January 17 indicates the path along which the opposite polarity flux had been canceling since January 13. From 03:58 UT on January 16 to 03:01 UT on January 18, approximately 9.2×10^{21} Mx of unsigned flux was removed from the photosphere by flux cancellation. The average rate of flux disappearance in cancellation is 3.6×10^{16} Mx s^{-1} . The flux cancellation continued to January 20. The X7.1 flare had one flare ribbon overlapping on the site of flux cancellation in the main flare phase.

In Figure 1, the magnetograms are drawn on top of the sunspot maps. When the AR was close to the disk center, the weight centers of magnetic flux coincide with the sunspot umbrae. However, when the AR moved to the west limb, the weight centers are shifted from the sunspot umbrae by projection effects. Although this effect has been well known, in Figure 2 we demonstrate the effect by a simple schematic drawing, and explore an intuitive analysis to untangle the projection effect on the observed magnetograms. In the figure, the solar surface is shown by the horizontal gray bar and the local normal at the observed point in the center is straight up. The long arrow

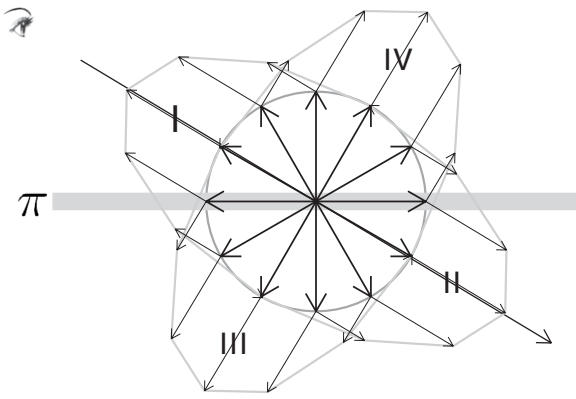


Figure 2. Schematic drawing of projection effects on the observed magnetic fields. The observation refers to the central point whose magnetic vector may point to any directions, highlighted by dark arrows. The LOS is shown by a long arrow. The gray arrows are observed components of magnetic field along and perpendicular to the LOS. The outer gray contours define four zones that represent different distributions of observed components in the vector magnetograms (see the interpretation in Table 2).

Table 2
Appearance in the Observed Vector Magnetograms

	IV∩I	I∩III	III∩II	II∩IV
B orientation (deg)	59–149	149–239	239–329	329–59
LOS	Positive	Positive	Negative	Negative
TRS	Limb-ward	Disk-ward	Disk-ward	Limb-ward

represents the LOS direction, which crosses the local normal at an angle of approximately 59° (or 0.33π). The magnetic vector, **B**, at the central point can be in any direction from 0° to 360° (2π). The projection of **B** on the LOS will appear as the positive (or negative) LOS component in the observed vector magnetograms when the **B** vector points to (or away from) the observer. On the other hand, the projection of **B** on the direction perpendicular to the LOS will appear as the limb-ward (or disk-ward) TRS field when the **B** vector points up (or down) referring to the LOS. The orientation of **B** can be grouped into four zones, Zones I, II, III, and IV, each of which has a span of π and is centralized at 0.83π (149°), 1.83π (329°), 1.33π (239°), and 0.33π (59°), respectively. The central two bins of Zones I and II, representing mostly the true HFs, dominantly contribute to the LOS fields in the observed vector magnetograms, while the central two bins of Zones III and IV, representing mostly the true vertical fields, contribute to the TRS fields in observations. Thus, in the observed vector magnetograms of 2005 January 20, the LOS fields dominantly come from the true HFs.

By following the history of continuous magnetic evolution shown in Figure 1, we mostly know the polarity of the observed magnetic features. With the knowledge of the magnetic polarity, then, we can judge how the true field components appeared in the observed vector magnetograms, and what true fields were shown by the LOS and TRS magnetograms, respectively. For clarity, we briefly summarize the appearance of various field components in the observed vector magnetograms in Table 2. It is of particular importance to notice that the observed LOS fields dominantly represent the true HFs without 180° ambiguity in field azimuth. For instance, the apparent stronger, positive LOS fields would mostly represent the HFs directed to the disk center, whereas the apparent negative LOS fields

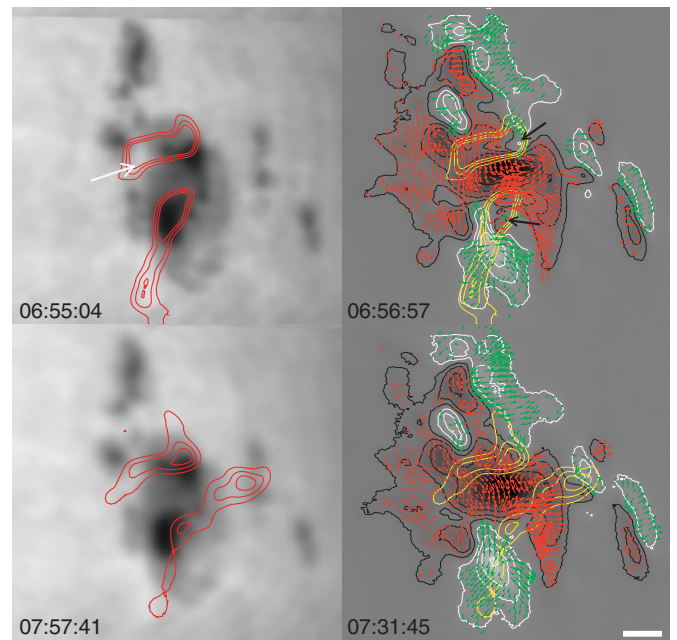


Figure 3. Left panels: $H\beta$ flare ribbons at 06:55 and 07:57 UT are contoured on the gray maps of the sunspot. The contour levels are 1.5, 3.6, and 5.8 times the background brightness. A white arrow indicates a flaring patch in the photospheric Fe I 5324 Å line; Right panels: Huairou vector magnetograms of 06:56 and 07:31 UT, superposed with flare ribbons. Two black arrows indicate the polarity reversal in the LOS magnetograms, which is induced by the flare emission.

(A color version of this figure is available in the online journal.)

represent the HFs to the limb (compare Figure 2 and Table 2). Note that for the sunspot distribution of AR 10720, either the westward or the eastward HFs are in a clearly sheared configuration. Therefore, the enhanced and weakened HFs in the east–west direction would represent the increase and decrease of magnetic shear, respectively, too. This fact will be utilized in this approach to explore what changes in the horizontal magnetic fields can be identified in the course of the X7.1 flare by studying the apparent variation in the LOS magnetograms.

To diagnose the true magnetic changes, the observed vector magnetograms have also been transformed into a heliographic coordinate system, although the transformation is not recommended when the AR is more than 50° away from disk center.

In Figure 3, the appearance of the X7.1 flare in $H\beta$ line is shown at approximately the flare maximum and declining phases. In the upper-left panel, an arrow indicates a flaring patch in the photospheric Fe I 5324 Å line. One ribbon of the $H\beta$ flare almost completely overlaps the strong positive sunspot. This seems to be consistent with an early finding that the close association between localized high-energy flare and changing sunspot umbra is a necessary condition for high-energy particles (McKenna-Lawlor 1970). In the magnetogram of 06:56 UT, two arrows indicate the flare-induced signals in the form of polarity reversal in small areas, the “flare anomaly” which was located inside the flare kernel emissions and sunspot umbrae. The reversal recovered after the impulsive phase of the flare (see the magnetograms at 07:31 UT in the lower-right panel). Interestingly, the emission in the photospheric Fe I 5324 Å line in the quiet photosphere did not cause any polarity reversal or other peculiar appearances in the magnetic signals.

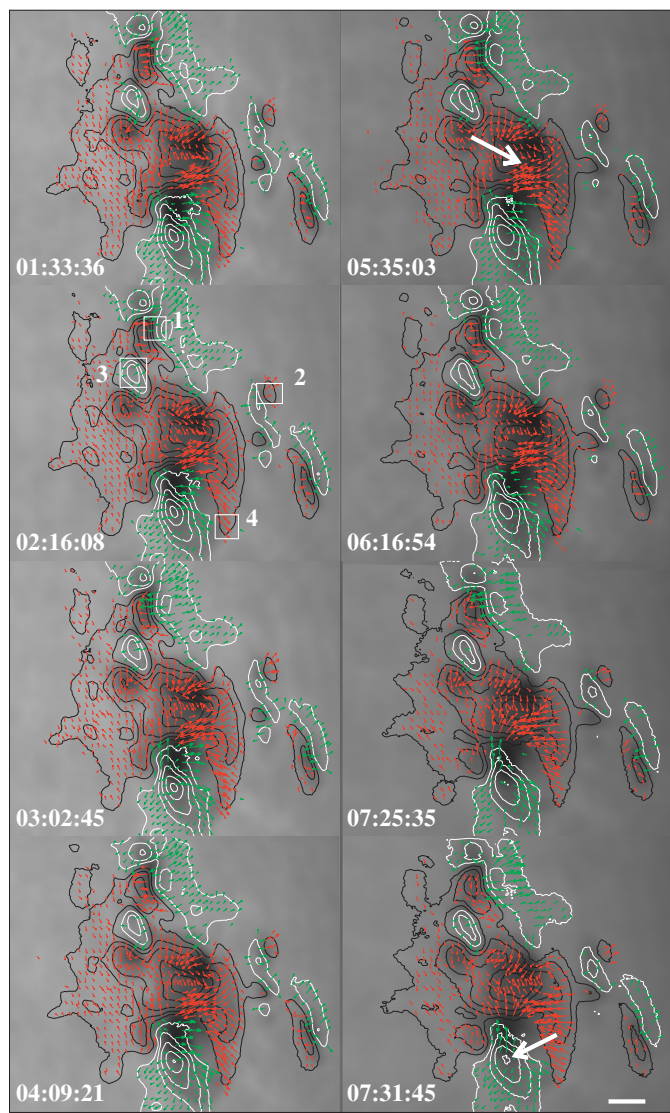


Figure 4. Time sequence of vector magnetograms on 2005 January 20, showing the pre-flare state and flare-associated changes. The presentation style for this figure is the same as that of Figure 1. The four boxes in the magnetograms of 02:16 UT mark control regions showing the sensitivity variation of the observed LOS magnetograms.

(A color version of this figure is available in the online journal.)

3. MAGNETIC CHANGES IN THE FLARE COURSE

3.1. Rapid Changes Seen from the Observed Vector Magnetograms

The pre-flare state and flare-associated changes in the magnetic fields are shown by the time sequence of observed vector magnetograms in Figure 4. In an interval of approximately 7 hr, the basic magnetic structures remained. From 01:33 to 07:31 UT, the relatively weak flux features outside of the δ -sunspots are mostly kept the same, either in appearance or in flux density. In the magnetogram at 02:16 UT, four control regions are framed by boxes and numbered from “1” to “4.” They are selected in locations outside of the δ -sunspot and deviated from flare ribbons, having approximately the same size as the patches with rapid magnetic changes in the flare course (see the following description). The unsigned mean flux densities in the four control regions are 220 ± 11 , 94 ± 7 , 163 ± 8 , and 74 ± 3 G, respectively,

in the observed interval. The standard deviations are 10–20 times smaller than the mean flux density.

While many magnetic features remained the same in both appearance and flux density, apparently pre-flare evolution can be seen from the time sequence of the observed vector magnetograms in Figure 4. Here, we only describe changes that can be visualized easily, and leave a more quantitative description to later paragraphs.

An obvious pre-flare evolution was shown by the positive LOS flux related to the main positive sunspot of the AR (indicated by an arrow at 07:31 UT). It had been gradually weakening since 01:34 UT in the LOS flux density. Evidently, its deepest contour of the flux density, referred to as 1500 G, had already disappeared, and the area of the second deepest contour, referred to as 1000 G, had greatly reduced. According to the list in Table 2, this evolution dominantly represents the weakening of HFs directed to the east. The weakening can be caused either by the reduction in the horizontal field strength, or by changing the azimuth to a more potential configuration. There are other gradual changes in the magnetograms that are not as easy to visualize.

An interesting feature of TRS fields in the magnetograms is shown by the arrow at 05:35 UT. It is characterized by enhanced TRS fields with some conflicting azimuth. Later, after the flare, obvious changes of the TRS fields are witnessed. According to the geometric analysis (see Table 2 and Figure 2), the enhanced TRS field segments dominantly represent the growth and evolution of a new EFR in the true vertical fields.

In this study, we concentrate on the rapid magnetic changes in the course of the flare. For the sake of credibility, we choose two sets of vector magnetograms to compare. One was taken at 06:16 UT, before the flare, and the other at 07:31 UT, after the flare. Considering the flare-induced abnormality in the form of polarity reversal (see the magnetograms at 06:56 UT in Figure 3), which was suggested to result from particle precipitation in the impulsive phase of the major flare (Ding et al. 2002), we avoid using the magnetograms taken during the flare. We subtract the post-flare vector magnetograms from the pre-flare magnetograms, and obtain the difference magnetograms of LOS and TRS fields, which are shown by yellow and blue contours in the upper-left and upper-right panels of Figure 5, respectively.

Both the LOS and TRS components show significant changes during the flare, and most of the changes took place in association with the δ -sunspots and flare ribbons. Because the sensitivity of the LOS magnetogram is roughly one order of magnitude higher than those of TRS magnetograms, in this study we focus on the rapid magnetic changes in the LOS component of the magnetic field.

It is remarkable that clear strengthening of observed LOS fields appears in the magnetic neutral zone between two major sunspots of opposite polarity. In addition, the outskirts of the δ -sunspots displayed a few isolated patches of weakened LOS fields. All the patches of unsigned flux changes above 100 G are numbered and marked from “1” to “10” in the difference sunspot image of 07:53–06:16 UT. As illustrated in Figure 2 and summarized in Table 2, the observed changes in LOS magnetograms, in fact, dominantly represent the physical changes in the true horizontal magnetic fields. Moreover, the 180° ambiguity in the observed field azimuth is no longer a serious problem from the close-limb LOS magnetogram observations. To summarize, for the first time, we have detected definitively the enhancement of sheared HFs, which are free of 180° ambiguity in field azimuth, in an extended area centralized

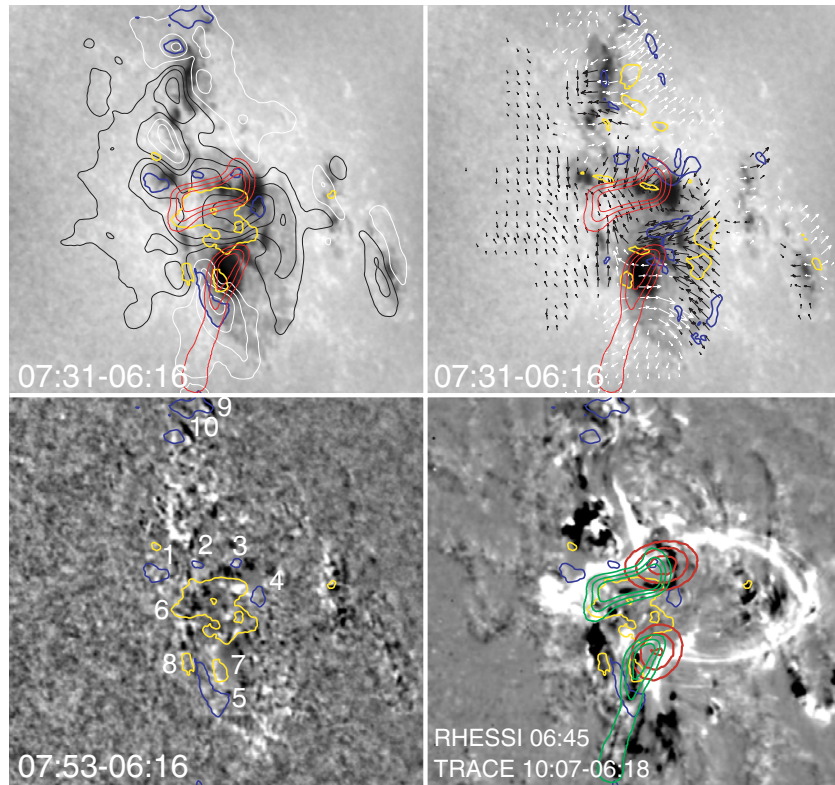


Figure 5. Upper-left panel: LOS magnetogram at 06:16 UT with superposition of magnetic changes in the LOS component from 06:16 to 07:31 UT. The yellow (blue) contours represent the rapid increase (decrease) in magnetic flux above 100 G. Upper-right panel: TRS magnetograms at 06:16 UT with superposition of magnetic changes in magnitude of the TRS components. The yellow (blue) contours represent the rapid increase (decrease) of TRS fields above 300 G. Lower-left panel: difference WL image from subtraction of image at 07:53 UT by that at 06:16 UT with superposition of LOS magnetic changes. Lower-right panel: difference 1550 Å image from a subtraction of the image at 10:07 UT from that at 06:18 UT with superposition of $H\beta$ flare ribbons (in green contours) and RHESSI hard X-ray sources (in red).

(A color version of this figure is available in the online journal.)

Table 3
Flux Changes in the Flare Course

Patch	Total Flux (10^{19} Mx)	Flux Density (Mx cm^{-2})
1	-5.51 ± 1.01	-109 ± 31
2	-1.38 ± 0.30	-93 ± 20
3	-1.30 ± 0.26	-99 ± 12
4	-3.47 ± 0.58	-119 ± 40
5	-12.62 ± 2.09	-121 ± 41
6	58.52 ± 7.57	155 ± 68
7	3.66 ± 0.57	128 ± 35
8	2.69 ± 0.50	107 ± 21
9	-8.37 ± 1.39	-120 ± 30
10	-3.43 ± 0.57	-120 ± 44

at the magnetic neutral line, and the reductions in sheared HFs at a few patches in the δ -sunspot outskirts.

The quantitative measurements of the rapid magnetic changes in terms of total flux and average flux density are detailed in Table 3. The reduction of total flux falls in the range of $(1.3\text{--}12.6) \times 10^{19}$ Mx, while the enhancement of total flux in the neutral zone is over 5.8×10^{20} Mx. The error scope of the total flux changes is estimated by assuming a sensitivity of 20 G for the LOS field measurement. The mean flux density change is 117 ± 17 G (Mx cm^{-2}) in the 10 marked patches, which is much higher than the detection limit.

To understand the physics, we try to connect the rapid magnetic changes with the more gradual pre-flare magnetic

evolution. The flux density evolution in the 10 selected patches is displayed in Figure 6 in comparison with the flux changes in the four control regions. Flux changes in Patch 7 are identified to be flare transient in nature. The flux density dropped impulsively during the flare impulsive phase, and then rapidly recovered after the impulsive phase. For most other patches, e.g., Patches 1, 2, 3, 5, 8, and 9, the flux changes consistently with the more general trend of pre-flare evolution (at least 1 hr before the flare), but rapidly when the flare impulsive phase began. For Patches 4, 6, and 8, the rapid magnetic changes only take place during the flare.

The great enhancement of HFs centralized on the neutral line is not easy to interpret uniquely. It might be caused by: (1) the field geometry changes toward more sheared configuration, or (2) the new emergence of pre-twisted flux, and/or (3) the magnetic flux cancellation among co-aligned flux threads in the neutral zone. The latter alternative seems to be consistent with the general evolution of the AR since 2005 January 13 (see Figure 1). The “head-to-tail” reconnection of co-aligned magnetic threads in the flux cancellation might result in the enhancement of horizontal magnetic fields and shear, as well as the formation, episodic strengthening, and brightening of the lower lying twisted “rope.” An interesting question is whether or not this reconnection among the core fields in the lower atmosphere could also cause the outer loop eruptions in some unpredicted ways.

We may account for the observed rapid magnetic changes in the outskirts of the AR by a geometric change of the magnetic

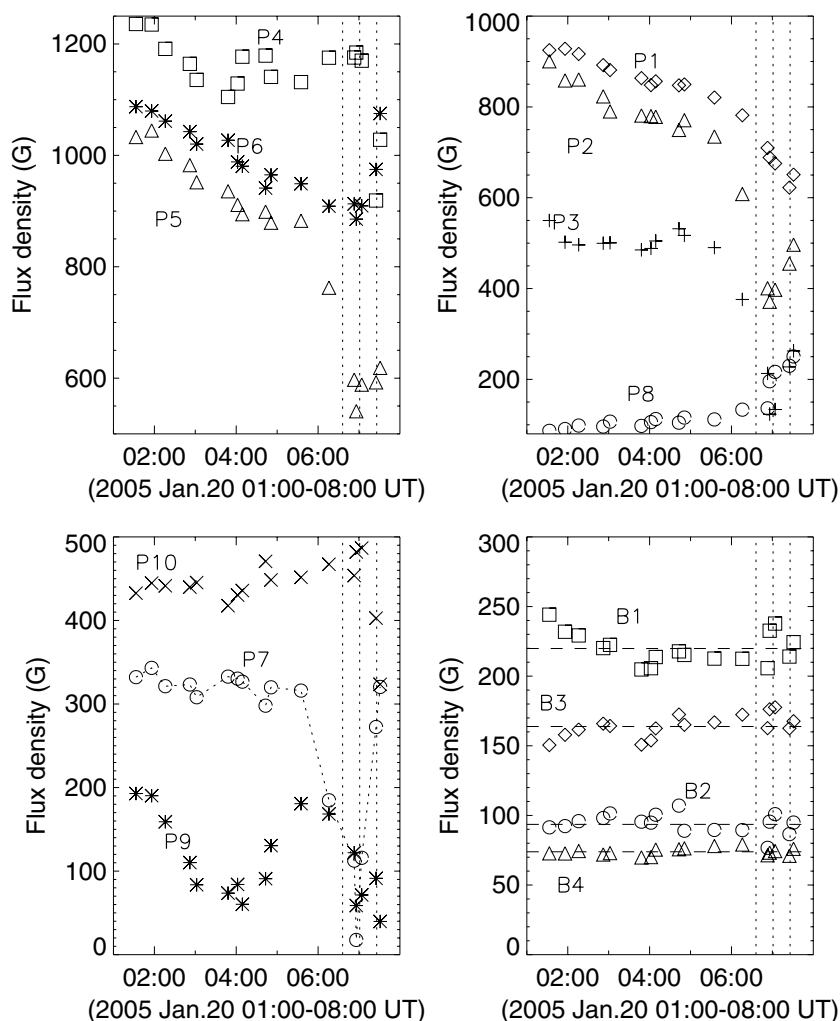


Figure 6. Magnetic flux changes in the 10 patches that show rapid magnetic changes during the flare and the four control regions marked by the boxes in Figure 4. The three vertical dotted lines mark the flare starting, maximum, and ending time, respectively.

vector. Assume an intrinsic field strength of 1 kG and a reduction of 100 G in the HF; then the magnetic vector should change by 6:4, 7:6, and 10:0 to a more vertical direction if its original orientation to the solar surface is 60°, 45°, and 30°, respectively.

The observed TRS fields display rapid magnetic changes as well. The patches contoured in the upper-right panel of Figure 5 are locations of changes above 250 G in the TRS fields. The changes fall into the range of 5×10^{19} to 2×10^{20} Mx but have rather big uncertainties that amount to 30% of the total changes. As discussed before, the changes dominantly come from the true vertical components of magnetic vectors in rapid flux emergence and cancellation.

The temporal coverage of vector magnetogram observations prohibits a verdict on whether the observed magnetic changes are permanent. However, permanent changes are implied by the structural changes of the δ -sunspot and transition region loops.

3.2. Structural Changes in Sunspots and UV/EUV Loops

Additional attestation to the detected HF changes is implied by the structural changes of the sunspot and transition region loops in the flare. It is noticed that the enhancement of HFs centralized on the neutral line is grossly correlated with the darkening of inner penumbrae in the δ -sunspots, while the decrease of HFs in the sunspot outskirts is consistent with the weakening of penumbrae there too (see the WL difference

image of 07:53–06:16 UT in the lower-left panel of Figure 5). Consistent with the earlier reports (Wang et al. 2002a, 2002b, 2004b; Deng et al. 2005; Liu et al. 2005; Chen et al. 2007), the sunspot structure changes for this event started immediately after the flare and were maintained for many hours later.

The magnetic fields in the vicinity of the magnetic neutral line are likely to be strongly sheared. This is hinted at by the UV structures shown in the 1550, 1600, and 1700 Å images in the magnetic neutral zone between two major sunspots. The UV fibril structures seem to depict structures of a magnetic flux “rope” in the neutral zone, which is illustrated by the time sequence of 1550 Å images in Figure 7 (see also the 1550 Å UV difference image of 10:07–06:18 UT in the lower-right panels of Figure 5). Although the *TRACE* images are vitiated by the “snow storm” caused by particle beating, by scrutinizing the *TRACE* movies made at 1550, 1600, and 1700 Å images, we could clearly identify the lower lying magnetic “rope” between two major sunspots, which did not erupt but were always being disturbed. However, the outer loops connecting to developing flare ribbons grew impulsively and erupted in the flare process.

In the image of 03:45 UT of Figure 7, the flux “rope” is outlined by thin red curves. The same curves are also marked in the two later images, indicating the persistent appearance of the lower lying rope structures. The earliest brightening of the flare could even be traced back to the interval of 05:38–05:58 UT at

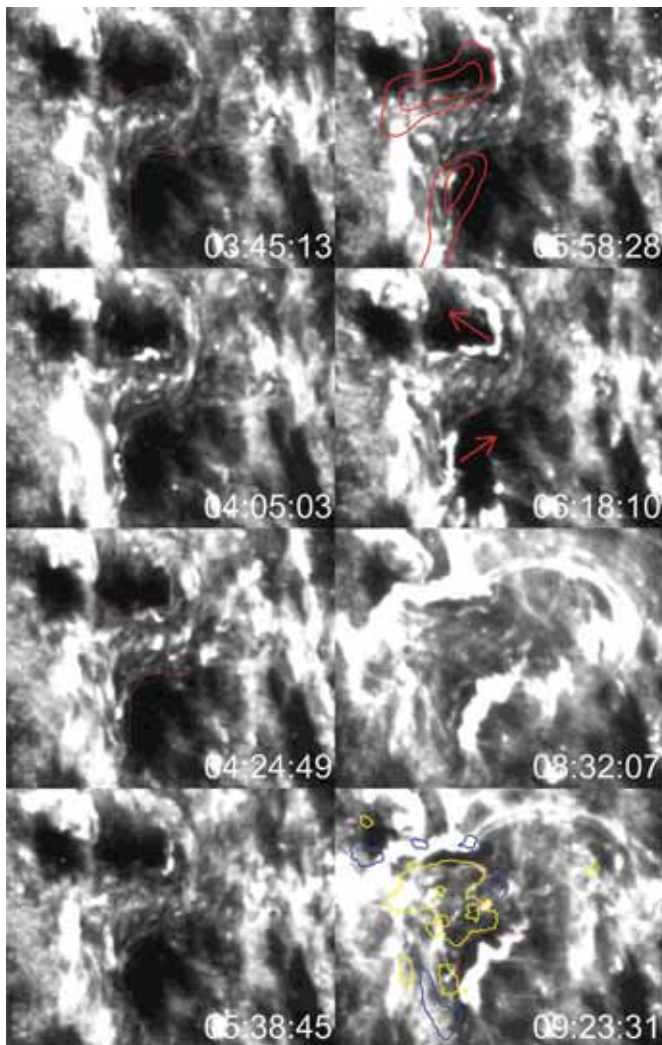


Figure 7. Time sequence of *TRACE* 1550 Å images. The two thin curves in red mark the position of magnetic rope structures between major sunspots of opposite polarities. $H\beta$ flare ribbons are superposed on the image at 05:58 UT by red contours. Rapid magnetic changes are superposed by contours on the image at 09:23 with the same style as in Figure 5. The earliest flaring in the flare started before 06:00 UT; the two red arrows indicate the growing and separating direction of the flare ribbons.

(A color version of this figure is available in the online journal.)

the edges of the rope structures. When the outer loops erupted after the flare, the lower lying rope remains, though disturbed and broadened slightly (see the images of 08:32 and 09:23 UT). This is a remarkable fact that a lower lying rope persists while the outer loops are erupting.

Interestingly, the rapidly enhanced HFs in Patch 6 coincide with the major part of the lower lying “rope,” and Patches “4” and “5,” with reduced HFs, coincide with footpoints of growing outer loops, as well as the RHESSI 250–500 keV nonthermal footpoint sources. If we assume that the transition region loops trace the magnetic lines of force, the upward expansion of UV loops would imply more vertical orientations of the magnetic fields, and thus weakening of HFs at their footpoints in the outskirts of δ -sunspots.

To understand the observed magnetic changes, we further examined the evolution of EUV structure from *SOHO*/EIT observations. Selected EIT 195 Å images from 03:00 to 06:36 UT, at which the flare impulsive phase started, are shown in Figure 8. Even before 03:00 UT, the outer loops of the AR

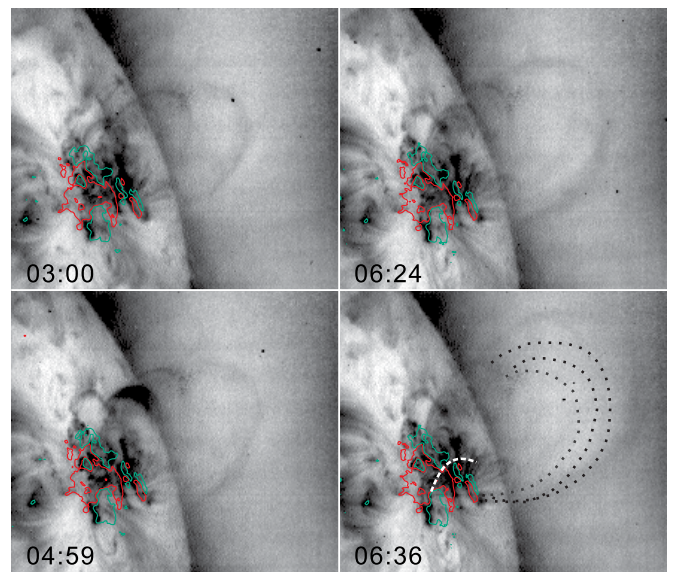


Figure 8. Selected EIT 195 Å images before the flare onset in the reversed color. MDI LOS magnetograms at the closest time are superposed on the images as contours of ± 200 G. Red (green) contours are for negative (positive) polarity, and the white dashed curve is the suspected magnetic neutral line. In the last panel, the positions of the earlier outer loops in the other panels are marked by black dotted lines. From 03:00 UT in each interval between two successive images, the upward expansion velocities are 1.3, 6.3, and 73.0 km s^{-1} , respectively.

(A color version of this figure is available in the online journal.)

began to slowly expand. Continuous expansion can be followed in the movies. Before 06:24 UT, the expansion velocity is less than 10 km s^{-1} ; however, about 10 minutes before the flare impulsive phase, the outer loops expanded rapidly at a velocity of 70–80 km s^{-1} . They seemed to become more and more vertical during the accelerated expansion. While the outer loops were expanding, the lower rope-like structures in the neutral zone showed some broadening and intermittent brightening without remarkable changes in height. This fact seems to attest to a scenario that the outskirts fields of the AR rapidly expanded and possibly erupted while the sheared core HFs close to the neutral lines strengthened in place during the flare course.

3.3. A Rapidly Growing EFR and Input of Magnetic Free Energy

To further diagnose the magnetic changes, we transform the observed vector magnetograms from the image plan into the heliographic coordinate system by the algebra developed by Gary & Hagyard (1990). As the flaring AR was quite close to the west limb, the spatial sampling in observed magnetograms is poor, and the observed TRS fields are quite noisy. In transforming the observed vector magnetograms, we make a low-pass filter to remove the high-frequency noise, which corresponds to a variation in spatial scale smaller than 5–6 pixels (1 pixel = 0.3516 arcsec). Moreover, when quantitative analysis is taken in the study, we leave enough room for uncertainty.

In Figure 9, the deprojected vector magnetograms, i.e., the magnetograms viewed directly above the local solar surface, are drawn at four selected times. The out boundaries of the lower lying rope structures in 1550 Å are superposed in the magnetograms. It is clearly shown that the lower lying rope is co-spatial with a bundle of strong and enhanced HFs. More important, a rapidly growing EFR is found in association with

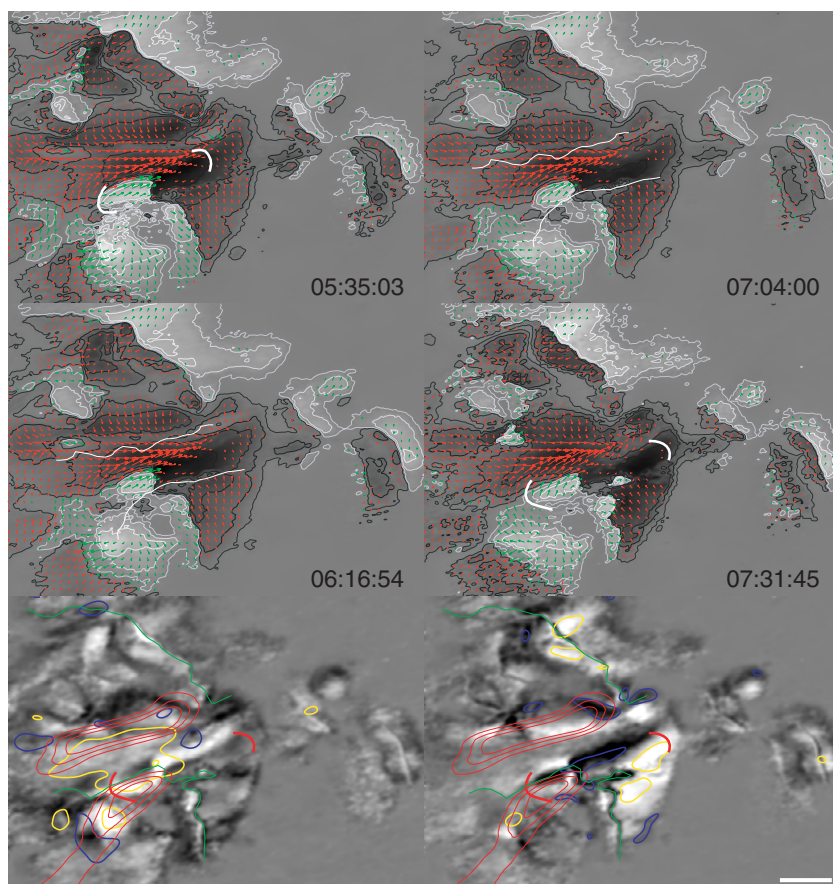


Figure 9. Selected vector magnetograms in the heliographic coordinate system (upper two rows), which are transformed from observed vector magnetograms. The red curves that mark the position of flux rope structure in Figure 7 are drawn by thin white lines in this figure. A rapidly growing EFR is marked by white brackets. In the lower-left panel, the changes of horizontal magnetic fields in the heliographic coordinate system during the flare are imaged from -300 to 300 G, in which the rapid magnetic changes revealed from the observed LOS magnetogram are superposed as in previous figures. In the lower-right panel, the changes of vertical fields are imaged from -500 to 500 G, with a superposition of TRS field changes obtained in the observed TRS magnetograms.

the enhanced HFs. For safety, we identify the EFR from the appearance of strong vertical fields, higher than 500 G. A bracket is drawn to mark the EFR according to the 1000 and 500 G isocontours for negative and positive polarities, respectively, in the magnetograms. From the rapid expansion of these contours, the EFR shows impulsive separation in the course of the flare from $06:16$ to $07:31$ UT.

In the lower-left and lower-right panels of Figure 9, the horizontal and vertical difference fields, respectively constructed from subtracting the deprojected magnetograms at $07:31$ UT from those at $06:16$ UT, are imaged in gray scales. When superposing the rapid magnetic changes in the LOS (TRS) component deduced from the observed vector magnetograms on top of the true horizontal (vertical) field changes, we confirmed our geometric analysis presented in Section 3.1. The observed LOS field changes are generally co-spatial with the true HF changes. The same is true for the observed TRS changes, which reflect the true vertical field changes. There is, indeed, a rapid enhancement of the true HFs in a large area sitting in the core of the δ -sunspots and some reduction in the sunspot's outskirts.

The development of the rapidly growing EFR is detailed in Figure 10. The flux measurements based on the deprojected magnetograms are noisy, but the general trend of the EFR's evolution is clear. The positive flux of the EFR shows a gradual increase at a rate of $2.87 \times 10^{16} \text{ Mx s}^{-1}$, while the negative flux decreases slowly. This appears to be typical for an EFR that emerged within a complex AR. From Figure 9, we know that the

negative flux of the EFR is free of an encounter with opposite polarity fields; however, the positive flux is continuously interacting and canceling with the pre-existing negative flux in its surroundings. However, neither the positive flux nor the negative flux displays rapid changes during the flare. The only impulsive change of the EFR during the flare is its separation of opposite polarity. Measured from the weight centers of 1000 and 500 G contours for the negative flux and positive flux, respectively, the EFR displayed an interesting behavior. The EFR's opposite polarities almost kept the constant separation of approximately $21,000$ km, and had not separated until the flare impulsive phase. Only after the impulsive phase, e.g., $06:16$ UT, do the EFR's opposite polarities initiate a rapid separation. The two fittings of the EFR's positions (see the two dashed lines in Figure 10) give a separating velocity of 2.4 and 4.3 km s^{-1} , respectively—much faster than that of a usual EFR. It is the rapid separation of the EFR that is co-temporal and, more or less, co-spatial with the great enhancement of the HFs during the flare.

To understand the true nature of the enhancement of the HFs in the core of the δ -sunspots, we calculate the magnetic nonpotentiality in terms of the free magnetic energy density in the photosphere (see Wang et al. 1996), which appears to outperform magnetic shear and other nonpotential parameters (Leka & Barnes 2007) in flare productivity. The free energy density distributions in pre- and after-flare phases are shown in contours superposed on the $H\beta$ images. As for the M1 flare with maximum at $04:35$ UT of 1990 August 30 (see Figure 5 in

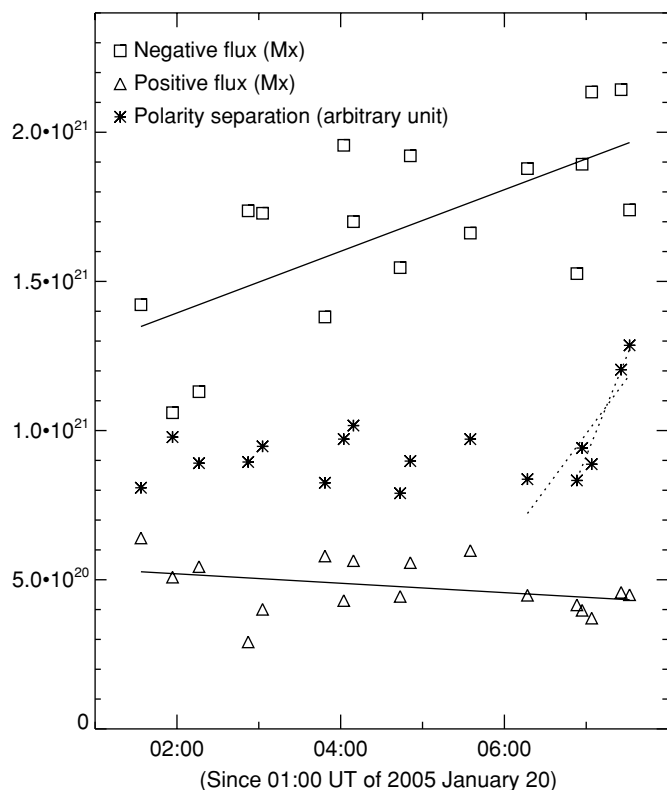


Figure 10. Flux and separation of the rapidly growing EFR marked in Figure 9. The flux measurements are made based on the vector magnetograms in the heliographic coordinate system. Though a bit more noisy in the measurements, the linear-square fittings shown by solid lines demonstrate the trend of the EFR's evolution. The EFR showed rapid separation during the flare. The two dotted lines that fit the weight centers of the opposite polarities roughly during the flare give a separation velocity of 2.4 and 4.3 km s⁻¹, respectively.

Wang et al. 1996), the region of high free energy is in between projections of two H β flare ribbons. Very rapid increase of magnetic free energy in the photosphere is obviously seen during the flare (see Figure 11). The total free energy within the contour of 2.5×10^4 erg cm⁻³ increased by 42% from 06:16 to 07:31 UT. The increase of free energy content during the flare reaches 1.03×10^{22} erg cm⁻¹. We have detected a sudden input of magnetic free energy in the photosphere in the course of the X7.1 flare. Assuming the nonpotentiality increases to a height of a few megameters (Jing et al. 2008), then the total free energy in the considered volume would be several times 10^{30} erg. The amount of free magnetic energy seems to be not enough for such a huge flare/CME event. We will discuss this fact in the last section.

The magnetic changes are not only limited in the region with high free magnetic energy. The AR has a dominantly negative helicity. Under the force-free assumption, the α_{best} by which the extrapolated vector fields best fit the observations in the photosphere can be taken as a proxy of magnetic helicity. The α_{best} shows a rapid enhancement from -2.5×10^{-6} Mm⁻¹ to -4.8×10^{-6} Mm⁻¹ during the flare. The magnetic fields of the AR in the photosphere become globally more complex during the flare.

4. CONCLUSION AND DISCUSSION

We find evidence that in the course of the X7.1 flare on 2005 January 20, there appeared a rapid enhancement of sheared horizontal magnetic fields in an extended area centralized on the magnetic neutral line, and a reduction of HFs in a few isolated

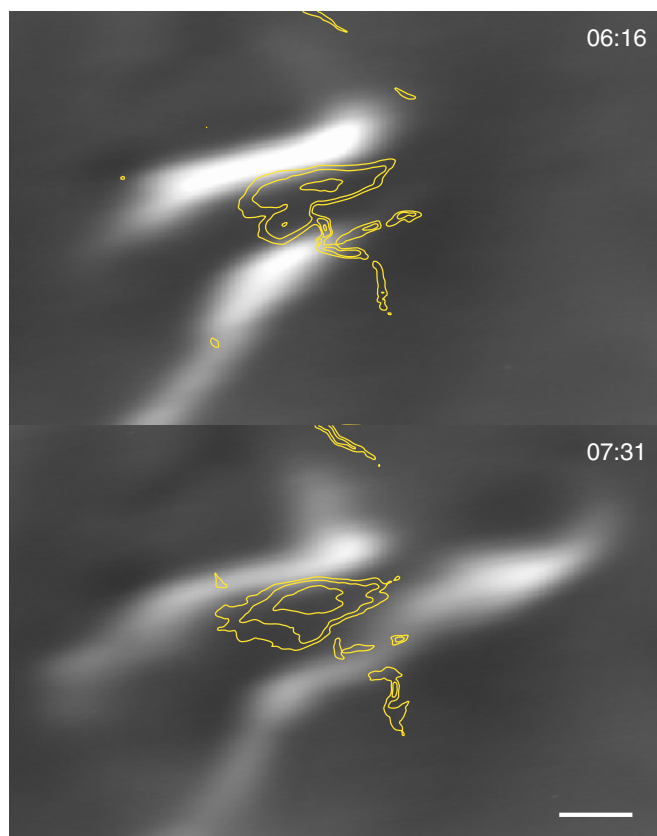


Figure 11. Free magnetic densities at 06:16 and 07:31 UT in the photosphere are superposed in the H β images at the closest time.

(A color version of this figure is available in the online journal.)

sites in the outskirts of the flaring AR. The detected magnetic changes are supported by the partial disappearance of outer penumbrae and darkening of inner penumbrae of the δ -sunspots, as well as the dynamics of UV/EUV loops. The characteristics of the rapid magnetic changes can be summarized as follows.

1. The rapid HF changes happen at the level of apparent flux density of 110–160 G and with total magnetic changes in the range of $(0.1\text{--}5.9) \times 10^{20}$ Mx in a few individual areas. Among them, the greatest enhancement of HFs is in the core of the δ -sunspot group and centralized on the magnetic neutral line.
2. The rapidly enhanced HFs in the AR core represent a sudden input of magnetic free energy in the photosphere. The free magnetic energy density increased by more than 40% during the flare. The area integration of free energy increase in the AR core is 10^{22} erg cm⁻¹ in order of magnitude.
3. The rapidly increased HFs centralized in the neutral line are closely associated with a “sheared” EFR, which had a total flux of more than 10^{21} Mx and displayed impulsive separation of opposite polarities at a speed of 2.4–4.3 km s⁻¹ during the flare.
4. The largely enhanced HFs in the core of the δ -sunspots coincide with a lower lying magnetic “rope” witnessed from TRACE 1550 Å structures. The lower lying rope episodically showed disturbance and brightening from long before to well after the flare, but never erupted in the course of the flare when the outer loops were growing and erupting.

It is well known that the standard flare model (see Hirayama 1974) does not predict any changes of magnetic fields in

the photosphere during flares. Moreover, for most, if not all, theoretical flare models, it has been assumed that the photospheric magnetic field “arises from photospheric or sub-photospheric currents and is invariant during a flare” (Priest & Forbes 2002, page 317).

Correctly grasping the key nature of flux cancellation, van Ballegooijen & Martens (1989) suggested that the reconnection at the magnetic neutral line would create the helical fields, implying the enhancement of HFs along the magnetic neutral line (see the three-dimensional view of magnetic configuration in their Figure 6). The idea has been developed further for bipolar and quadrupole configurations (see Amari et al. 2007). Backed by the vector magnetogram analysis, Wang & Shi (1991, 1993) identified the first evidence of magnetic reconnection in the photosphere. They proposed a two-step reconnection model to interpret the association between the flux cancellation and the flare. They suggested that the slow magnetic reconnection at the site of flux cancellation would finally result in fast and explosive reconnection in the corona, which is directly responsible for the free energy release in flares. Although this conceptual model confronts the observed magnetic changes in the photosphere, its phenomenological nature prevents it from quantifying the detailed magnetic changes. Moore et al. (2001) also incorporated the magnetic reconnection in the lower atmosphere into their tether-cutting flare/CME model. The model may correctly imply the likely enhancement of horizontal magnetic fields crossing the neutral line in the photosphere, but prefers a relaxation of magnetic shear after the first step of reconnection in the photosphere. All the above models adopt an idea of two-step magnetic reconnection in flares, and emphasize the importance of reconnection in the lower atmosphere, which would possibly result in the enhancement of HFs close to the magnetic neutral lines.

The magnetic breakout model (Antiochos et al. 1999) does suggest the strong sheared core fields in the center of the overall quadrupole magnetic structure and the breakout of outskirts magnetic fields. This model correctly predicts the reduction of outskirts HFs, as do the other models, e.g., the various two-step reconnection models. Zhang et al. (2006) supplemented the magnetic breakout model with an idea of two current sheets reconnection in interpreting the behavior of interdependent flare/CME. In their model, one current sheet lies horizontally above the overall quadrupolar flux system, another is vertical in the interior of the flux system and below the catastrophic flux rope. And, indeed, external and internal reconnection in flares has been reported earlier by Sterling & Moore (2001). However, the magnetic breakout model does not predict whether the sheared core is continuously strengthening in the photosphere, or weakening when it transferred the helicity into the overall erupted fields.

Each individual flare model provides some useful guide to understand some key part of the multi-aspect observations; however, the observed rapid magnetic changes during this extremely high energy flare could not be correctly predicted by any single flare/CME model. The rapid magnetic changes reported here, amongst many other convincingly reported examples, provide new clues and add further constraints on flare/CME theories. Although it is still premature to propose a complete picture for the magnetic energy storage and impulsive release in this and other major flares, the current observations of flare magnetism clearly point out some key elementary ingredients in flare physics. They are: (1) a set of strongly sheared HFs in the core of a complex δ -sunspot group, which is manifested as a lower lying flux rope above the magnetic neutral zone; (2) a sudden input of magnetic

free energy in the core fields in the form of rapidly enhanced HFs; (3) rapid growth of a sheared EFR along the magnetic neutral line and its associated magnetic reconnection in the lower solar atmosphere, which is responsible for the sudden input of magnetic free energy; (4) a gradual expansion of outer loops before the flare and catastrophic eruption after the flare impulsive phase; and (5) a lower lying flux rope that showed episodic disturbance, brightening, and/or growth, but never erupted during the flare. We are not aware if the last element is particular only for this flare or typical for other major flares also.

The observed rapid magnetic changes in the core HFs in this work and a few previous studies seem to have more bearing on the mechanism or mechanisms of flare triggering. We tentatively propose a conceptual model of flare triggering. It consists of the following key scenarios: (1) the strong sheared HFs, manifested as a lower lying flux rope, get rapid enhancement by sudden input of magnetic free energy by means of rapid growth of an EFR and/or magnetic reconnection in the vicinity of the magnetic neutral line close to the photosphere; (2) unlike what was previously thought, the strengthening lower lying flux rope does not erupt but pushes the overlying magnetic structure together with the current sheet (or current concentration) in the magnetic interface elevate rapidly into higher corona; (3) in the higher corona, the current sheet meets the condition of abnormal resistivity and becomes unstable, so that rapid magnetic reconnection takes place to impulsively release magnetic energy in a flare; and (4) the violent and rapid reconnection itself creates a large-scale flux rope which escapes from the solar corona in the form of a CME. This model suggests that it is the coupling between photosphere and corona that triggers the explosive flare and CME. It does not rely on the prerequisite of a flux rope in the higher corona, which differentiates our model from the traditional flux rope models. It does not require an expulsion of core-sheared fields into the high corona, which differentiates it from the magnetic breakout. Detailed numerical simulation is undertaken to verify the conceptual model.

More major flare/CME events need to be examined to determine if the magnetic changes revealed in the course of flares by this study are common. Recent progress in observations of flare-associated magnetic changes seems already to appeal to more reliable models of flare/CMEs, which could confront greatly improved observations.

We are grateful to the *SOHO* MDI and EIT, *TRACE*, *HSOS*, and *BBSO* teams for the good data used in this study. This work is supported by National Key Basic Program of China (2006CB806303) and National Natural Science Foundation of China (10573025, 10603008, 10703007, 10873020).

REFERENCES

- Amari, T., Aly, J. J., Mikic, Z., & Linker, J. 2007, *ApJ*, **671**, L189
 Antiochos, S. K., DeVore, C. R., & Klimchuk, J. A. 1999, *ApJ*, **510**, 485
 Bruzek, A. 1967, *Sol. Phys.*, **2**, 451
 Bumba, V. 1987, in Proc. 10th IAU European Regional Astron. Meeting, Vol. 1 (Ondrejov, Czechoslovakia: Czechoslovak Academy of Sciences), 59
 Canfield, R. C., et al. 1993, *ApJ*, **411**, 362
 Chen, W., Liu, C., Song, H., Deng, N., Tan, C., & Wang, H. 2007, *Chin. J. Astron. Astrophys.*, **7**, 733
 Cameron, R., & Sammis, I. 1999, *ApJ*, **525**, L61
 Delaboudinière, J.-P., et al. 1995, *Sol. Phys.*, **162**, 292
 Deng, N., Liu, C., Yang, G., Wang, H., & Denker, C. 2005, *ApJ*, **623**, 1195
 Ding, M. D., Qiu, J., & Wang, H. 2002, *ApJ*, **576**, L83
 Ding, Y., Hagyard, M. J., Deloach, A. C., Hong, Q. F., & Liu, X. P. 1987, *Sol. Phys.*, **109**, 307

- Falconer, D. A., Moore, R. L., & Gary, G. A. 2006, *ApJ*, **644**, 1258
- Gaizauskas, V., & Švestka, Z. 1987, *Sol. Phys.*, **114**, 389
- Gary, G. A., & Hagyard, M. J. 1990, *Sol. Phys.*, **126**, 21
- Giovanelli, R. G. 1939, *ApJ*, **89**, 55
- Hagyard, M. J., Smith, J. B., Jr., Teuber, D., & West, E. A. 1984, *Sol. Phys.*, **91**, 115
- Handy, B. N., et al. 1999, *Sol. Phys.*, **187**, 229
- Hirayama, T. 1974, *Sol. Phys.*, **34**, 323
- Jing, J., Wiegmann, T., Suematsu, Y., Kubo, M., & Wang, H. 2008, *ApJ*, **676**, L81
- Kosovichev, A. G., & Zharkova, V. V. 1999, *Sol. Phys.*, **190**, 459
- Kosovichev, A. G., & Zharkova, V. V. 2001, *ApJ*, **550**, L105
- Kubo, M., et al. 2007, *PASJ*, **59**, s779
- Leka, K. D., & Barnes, G. 2007, *ApJ*, **656**, 1173
- Li, J. P., Ding, M. D., & Liu, Y. 2005a, *Sol. Phys.*, **229**, 115
- Li, J., Mickey, D. L., & LaBonte, B. J. 2005b, *ApJ*, **620**, 1092
- Lin, Y., & Gaizauskas, V. 1987, *Sol. Phys.*, **109**, 81
- Liu, C., Deng, N., Liu, Y., Falconer, D., Goode, P. R., Denker, C., & Wang, H. 2005, *ApJ*, **622**, 722
- Liu, Y., Jiang, Y., Ji, H., Zhang, H., & Wang, H. 2003, *ApJ*, **593**, L137
- Livi, S. H. B., Wang, J., & Martin, S. F. 1985, *Aust. J. Phys.*, **38**, 855
- Lü, Y., Wang, J., & Wang, H. 1993, *Sol. Phys.*, **148**, 119
- Martin, S. F., Livi, S. H. B., & Wang, J. 1985, *Aust. J. Phys.*, **38**, 929
- McKenna-Lawlor, S. M. P. 1970, *ApJ*, **159**, 51
- Meunier, N., & Kosovichev, A. 2003, *A&A*, **412**, 541
- Moore, R. L., Sterling, A. C., Hudson, H., & Lemen, J. R. 2001, *ApJ*, **552**, 833
- Moreton, G. E., & Severny, A. B. 1968, *Sol. Phys.*, **3**, 282
- Patterson, A. 1984, *ApJ*, **280**, 884
- Patterson, A., & Zirin, H. 1981, *ApJ*, **243**, L99
- Qiu, J., & Gary, D. E. 2003, *ApJ*, **599**, 615
- Ramsey, H. E., & Smith, S. F. 1963, *ApJ*, **68**, 290
- Priest, E. R., & Forbes, T. G. 2002, *Ann. Rev. Astron. Astrophys.*, **10**, 313
- Rust, D. M. 1976, *Sol. Phys.*, **47**, 21
- Rust, D., Sakurai, T., Gaizauskas, V., Hofmann, A., Martin, S. F., Priest, E. R., & Wang, J. 1994, *Sol. Phys.*, **155**, 69
- Sakurai, T., & Hiei, E. 1996, *Adv. Space Rev.*, **17**, 91
- Scherrer, P. H., et al. 1995, *Sol. Phys.*, **162**, 129
- Schmieder, B., et al. 1994, *Sol. Phys.*, **150**, 199
- Schrijver, C. J. 2007, *ApJ*, **662**, L119
- Spirock, T. J., Yurchyshyn, V. B., & Wang, H. 2002, *ApJ*, **572**, 1072
- Sterling, A. C., & Moore, R. L. 2001, *J. Geophys. Res.*, **106**, 25227
- Sudol, J. J., & Harvey, J. W. 2005, *ApJ*, **635**, 647
- Švestka, Z. 1981, in *Solar Flare Magnetohydrodynamics* (New York: Gordon & Breach), 47
- Somov, B. 1985, *Sov. Phys. Usp.*, **28**, 271
- van Ballegoijen, A. A., & Martens, P. C. H. 1989, *ApJ*, **343**, 971
- Wang, H. 2007, in *ASP Conf. Series 369, New Solar Physics with Solar-B Mission*, ed. K. Shibata, S. Nagata, & T. Sakurai (San Francisco, CA: ASP), 449
- Wang, H., Ewell, M. W., Jr., Zirin, H., & Ai, G. 1994, *ApJ*, **424**, 436
- Wang, H., Ji, H., Schmahl, E. J., Qiu, J., Liu, C., & Deng, N. 2002a, *ApJ*, **580**, L177
- Wang, H., Spirock, T. J., Qiu, J., Ji, H., Yurchyshyn, V., Moon, Y. J., Denker, C., & Goode, P. R. 2002b, *ApJ*, **576**, 497
- Wang, H., Liu, C., Qiu, J., Deng, N., Goode, P. R., & Denker, C. 2004a, *ApJ*, **601**, L195
- Wang, H., Liu, C., Deng, Y., & Zhang, H. 2005, *ApJ*, **627**, 1031
- Wang, H., Liu, C., Jing, J., & Yurchyshyn, V. 2007, *ApJ*, **671**, 973
- Wang, H., Qiu, J., Jing, J., Spirock, T. J., Yurchyshyn, V., Abramenko, V., Ji, H., & Goode, P. R. 2004b, *ApJ*, **605**, 931
- Wang, J. 1998, in *ASP Conf. Series 140, Synoptic Solar Physics—18th NSO/Sacramento Peak Summer Workshop*, ed. K. S. Balasubramanian, J. Harvey, & D. Rabin (San Francisco, CA: ASP), 121
- Wang, J., & Li, W. 1998, in *ASP Conf. Series 150, New Perspectives on Solar Prominences*, Proc. IAU Colloq. 167, ed. D. F. Webb, B. Schmieder, & D. M. Rust (San Francisco, CA: ASP), 98
- Wang, J., & Shi, Z. 1991, *Acta Astrophys. Sin.*, **11**, 389
- Wang, J., & Shi, Z. 1993, *Sol. Phys.*, **143**, 119
- Wang, J., Shi, Z., Wang, H., & Lü, Y. 1996, *ApJ*, **465**, 861
- Yurchyshyn, V., Wang, H., Abramenko, V., Spirock, T. J., & Krucker, S. 2004, *ApJ*, **605**, 546
- Zhang, Y. Z., Wang, J. X., & Hu, Y. Q. 2006, *ApJ*, **641**, 572
- Zirin, H. 1972, *Sol. Phys.*, **22**, 34
- Zirin, H. 1988, *Astrophysics of the Sun* (Cambridge: Cambridge Univ. Press)
- Zirin, H., & Liggett, M. A. 1987, *Sol. Phys.*, **113**, 267